Monthly Notices
of the
ROYAL ASTRONOMICAL SOCIETY

MNRAS **462,** 2995–3005 (2016)
Advance Access publication 2016 August 1

doi:10.1093/mnras/stw1853

The mass-loss rates of red supergiants at low metallicity: detection of rotational CO emission from two red supergiants in the Large Magellanic Cloud

Mikako Matsuura,[1,2★] B. Sargent,[3★] Bruce Swinyard,[1,4†] Jeremy Yates,[1] P. Royer,[5] M. J. Barlow,[1] Martha Boyer,[6] L. Decin,[5,7] Theo Khouri,[7,8] Margaret Meixner,[9,10] Jacco Th. van Loon[11] and Paul M. Woods[12]

[1]*Department of Physics and Astronomy, University College London, Gower Street, London WC1E 6BT, UK*
[2]*School of Physics and Astronomy, Cardiff University, Queen's Buildings, The Parade, Cardiff CF24 3AA, UK*
[3]*Center for Imaging Science and Laboratory for Multiwavelength Astrophysics, Rochester Institute of Technology, 54 Lomb Memorial Drive, Rochester, NY 14623, USA*
[4]*RAL Space, Rutherford Appleton Laboratory, Chilton, Didcot, Oxfordshire OX11 0QX, UK*
[5]*Instituut voor Sterrenkunde, KU Leuven, Celestijnenlaan 200D B-2401, 3001Leuven, Belgium*
[6]*Observational Cosmology Lab, Code 665, NASA Goddard Space Flight Center, Greenbelt, MD 20771, USA*
[7]*Astronomical Institute Anton Pannekoek, University of Amsterdam, PO Box 94249, NL-1090GE Amsterdam, the Netherlands*
[8]*Onsala Space Observatory, Department of Radio and Space Science, Chalmers University of Technology, SE-43992 Onsala, Sweden*
[9]*Space Telescope Science Institute, 3700 San Martin Drive, Baltimore, MD 21218, USA*
[10]*Department of Physics and Astronomy, The Johns Hopkins University, 366 Bloomberg Center, 3400 N. Charles Street, Baltimore, MD 21218, USA*
[11]*School of Physical and Geographical Sciences, Lennard-Jones Laboratories, Keele University, Staffordshire ST5 5BG, UK*
[12]*Astrophysics Research Centre, School of Mathematics and Physics, Queen's University, University Road, Belfast BT7 1NN, UK*

Accepted 2016 July 22. Received 2016 July 22; in original form 2015 June 4

ABSTRACT

Using the PACS and SPIRE spectrometers on-board the *Herschel Space Observatory*, we obtained spectra of two red supergiants (RSGs) in the Large Magellanic Cloud (LMC). Multiple rotational CO emission lines (J = 6–5 to 15-14) and 15 H_2O lines were detected from IRAS 05280−6910, and one CO line was detected from WOH G64. This is the first time that CO rotational lines have been detected from evolved stars in the LMC. Their CO line intensities are as strong as those of the Galactic RSG, VY CMa. Modelling the CO lines and the spectral energy distribution results in an estimated mass-loss rate for IRAS 05280−6910 of 3×10^{-4} $M_\odot$ yr^{-1}. The model assumes a gas-to-dust ratio and a CO-to-H_2 abundance ratio is estimated from the Galactic values scaled by the LMC metallicity ([Fe/H] ~ -0.3), i.e. that the CO-to-dust ratio is constant for Galactic and LMC metallicities within the uncertainties of the model. The key factor determining the CO line intensities and the mass-loss rate found to be the stellar luminosity.

Key words: stars: AGB and post-AGB – circumstellar matter – stars: massive – stars: mass-loss – ISM: molecules – Magellanic Clouds.

1 INTRODUCTION

At the end of their lives, stars lose a large fraction of their mass from their surfaces. High-mass (>8 $M_\odot$) stars evolve into the red-supergiant (RSG) phase, and lose a large amount of mass through stellar winds. RSGs are considered to be the major progenitors of Type II-P supernovae (SNe) (Smartt 2009). High-mass stars lose a large amount of mass during the RSG phase, determining the RSG mass at the time of a SN explosion (Meynet et al. 2015). In order to fully understand post-main sequence stellar evolution, it is important to characterize the mass-loss processes of RSGs.

The hydrodynamical simulation of RSG mass loss is not yet fully modelled theoretically, but the basic mechanisms are believed to be the same as for asymptotic giant branch (AGB) stars, which are their lower mass evolutionary counterparts. AGB stars are more populous than RSGs and thus better investigated. It is widely accepted

★ E-mail: mikako@star.ucl.ac.uk (MM); sargent@stsci.edu (BS)
† Prof. Bruce Swinyard passed away on 2015 May 22. He was very passionate about science, engineering, with good sense of humour. He made tremendous efforts to make space missions successful, including the *Herschel Space Observatory*. This paper is dedicated to his memory. We will miss him.

© The Author 2016. Published by Oxford University Press on behalf of The Royal Astronomical Society. This is an Open Access article distributed under the terms of the Creative Commons Attribution License (http://creativecommons.org/licenses/by/4.0/), which permits unrestricted reuse, distribution, and reproduction in any medium, provided the original work is properly cited.

that stellar winds from RSGs and AGB stars are dust driven: stellar pulsations elevate some gas from the stellar surface, and from the levitated atmosphere dust grains are condensed (e.g. Höfner & Dorfi 1997). The dust grains experience radiation pressure from the central star, triggering outward movement. The dust motion drags the surrounding gas, driving stellar winds of both gas and dust.

Due to this dust-driven mechanism, the mass-loss rates from RSGs and AGB stars should depend on two major parameters: the luminosity of the central star, and the metallicity of the galaxy.

The luminosity of the central star determines the radiation pressure on the dust grains. Wachter et al. (2008) predicted that the mass-loss rate should correlate with luminosity. While Galactic RSGs have large uncertainties in measuring their luminosities, extragalactic RSGs have well-determined luminosities, as the distance to the stars can be adopted as the distance to the galaxy. With its close distance of 50 kpc (Pietrzynski et al. 2013), the Large Magellanic Cloud (LMC) can be used to study the impact on luminosity of mass-loss rates.

Secondly, the mass-loss rate is expected to approximately correlate with metallicity, which can be represented by the metallicity of the parent galaxy. RSG mass loss is driven by radiation pressure on dust grains (e.g. Justtanont & Tielens 1992). Dust grains from oxygen-rich stars are composed of metals, such as Fe, Si, O, Al, hence, a lower metallicity should result in a smaller mass of dust grains. For a lower dust mass, the integrated cross-section for radiation pressure on dust grains should reduce, resulting in a lower mass-loss rate at least for oxygen-rich stars (Bowen & Willson 1991). Indeed, Marshall et al. (2004) measured the expansion velocities of LMC RSGs, using OH masers, and found lower expansion velocities for LMC RSGs compared to their Galactic counterparts, suggesting a metallicity effect on the dust radiation-pressure driven mass-loss rate.

To date, studies of mass-loss rates in LMC RSGs have been based on their IR spectral energy distributions (SEDs; e.g. van Loon et al. 1999; Groenewegen et al. 2007; Sargent et al. 2010; Riebel et al. 2012), measuring their dust mass-loss rate, whereas historically, Galactic AGB stars and RSGs have been studied more intensively, using CO rotational lines (e.g. Knapp & Morris 1985; Ramstedt et al. 2008). Complementary studies of CO emission in the LMC RSGs are important.

With the aim of investigating the physics and chemistry of the circumstellar envelopes of evolved stars at low metallicity, we have measured molecular emission lines at far-infrared (IR) and submillimeter wavelengths, including CO rotational emission from two IR RSGs in the LMC. Additionally, H_2O lines have been detected. This is the first detection of CO rotational emission lines from RSGs in the LMC to our knowledge. We report the analysis of these molecular lines.

2 OBSERVATIONS AND DATA REDUCTION

We observed two RSGs with the *Herschel Space Observatory* (Pilbratt et al. 2010). The primary target, IRAS 05280−6910 was chosen because it is the brightest LMC RSG at far-IR wavelengths (Boyer et al. 2010), with a 250 μm flux of 205 mJy. Its mid-IR spectrum shows 10 μm silicate band in absorption with a peak of the SED at about 25 μm. OH and H_2O masers have been detected (Wood et al. 1992; van Loon et al. 2001). IRAS 05280−6910 was found towards the cluster NGC 1984 (van Loon et al. 2005b).

The second target is WOH G64, a well-known OH/IR star in the LMC (Elias, Frogel & Schwering 1986). This star has a strong silicate absorption in its mid-IR spectrum, accompanied by OH masers (Elias et al. 1986; Wood, Bessell & Whiteoak 1986; Roche, Aitken & Smith 1993). Based on mid-IR interferometric observations, Ohnaka et al. (2008) suggested the presence of a face-on torus around WOH G64. This is one of the most luminous mass-losing RSGs in the LMC, with a bolometric luminosity of ∼−9 mag (van Loon et al. 1999; Levesque et al. 2009)

The submillimeter spectrum of IRAS 05280−6910 was obtained, using the SPIRE Fourier Transform spectrometer (Griffin et al. 2010; Swinyard et al. 2010) on-board the *Herschel Space Observatory*. The data were acquired on 2012 June 16 and 17 (OBSID: 1342247097 and 1342247098) in a *Herschel* Open Time Program (OT1_mmatsuur_1). The total duration of the observation was 13752 s×2. The SPIRE FTS simultaneously covers the short wavelength band (SSW; SPIRE Short Wavelength Spectrometer Array; 190–313 μm; 957–1577 GHz) and long wavelength band (SLW; SPIRE Long Wavelength Spectrometer Array; 303–650 μm; 461–989 GHz), yielding a frequency coverage from 444 to 1540 GHz, with a spectral resolution of 1.2 GHz. The FTS sensitivity varies across the spectra, with the best sensitivity available region at about 700–800 GHz (Swinyard et al. 2014), corresponding to the CO $J = 6$–5 and 7–8 lines. Unfortunately, the SLW spectrum suffered from a temperature drift in the SPIRE detectors, so that the continuum level is unreliable. We discorded the spectrum below ∼700 GHz, and added some uncertainties to the SLW spectra above ∼700 GHz. The spectrum was reduced in HIPE version 11 (Ott 2010).

The PACS (Poglitsch et al. 2010) spectrum of IRAS 05280−6910 was obtained on 2013 March 19 (OBSID: 1342267866), in a *Herschel* Open Time Program (OT2_bsargent_1). The program targeted the 173 μm CO $J = 15$–14 and 186 μm CO $J = 14$–13 lines. The target CO lines were covered by the first-order grating with a resolving power of $R \sim 1500$, while the second-order grating covered the 92 μm H_2O 6_{43}–6_{34} line, with a resolving power of $R \sim 2000$. The chopped-nodded PACS range spectroscopy mode was used. The total duration of the observation was 2240 s.

PACS obtained the spectrum of WOH G64 on 2013 April 12 (OBSID: 1342269921), as part of the same programme (OT2_bsargent_1). The spectral setting was the same as that for IRAS 05280−6910, and the total observing time was 6712 s.

The PACS spectra were reduced with HIPE version 13. The absolute flux calibration was performed relative to the telescope background. Both targets were considered point-like, i.e. the fluxes were extracted from the central 'spaxel' only, inclining proper beam correction. Calibration set 65 was used for all reduction and calibration steps.

3 SPECTRA AND DETECTED MOLECULES

Fig. 1 shows the SPIRE spectrum of IRAS 05280−6910 in comparison to the spectrum of the Galactic RSG VY CMa (Royer et al. 2010; Matsuura et al. 2014). CO rotational lines and some strong H_2O lines are detected, with their line intensities and identifications summarized in Table 1.

The detected CO lines are displayed in Fig. 2. The spectra were fitted using sinc instrumental line shape (Naylor et al. 2014). A systematic velocity of 270 km s^{-1} for the LMC (Marshall et al. 2004) was adopted.

Our PACS programme targeted two CO transitions ($J = 14$–13 and 15–14) in the first grating order. As a bonus, the 92 μm H_2O line was detected in the second-order spectrum. Fig. 3 displays the spectra of IRAS 05280−6910 and WOH G64, showing

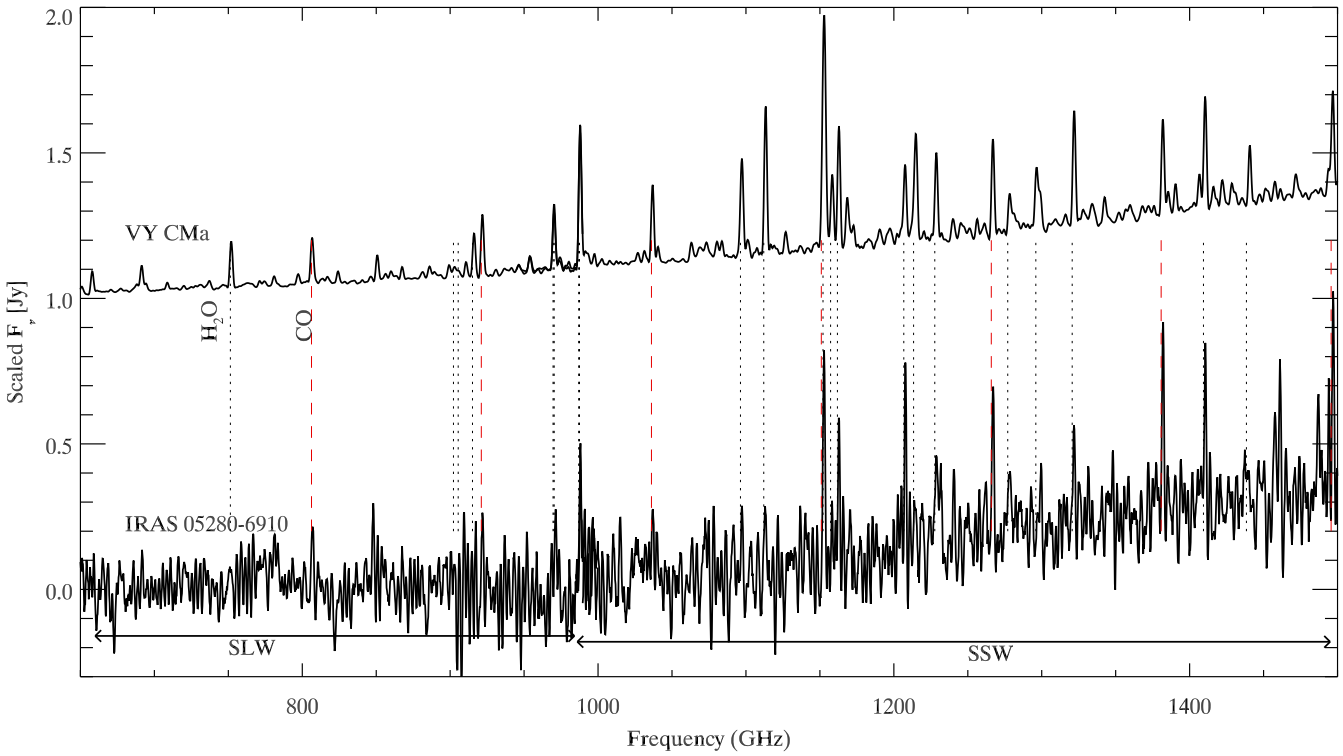

Figure 1. The SPIRE FTS spectra of the LMC red-supergiant, IRAS 05280-6910, compared with the SPIRE FTS spectra of the Galactic red-supergiant, VY CMa. The spectra were scaled for clarity. The spectrum of IRAS 05280−6910 is unapodized, with the detected lines appearing as sharp peaks, but with instrumental line shape of a sinc function included. The spectrum VY CMa was apodized, i.e. instrumental line shape was removed, but the spectral resolution was lowered.

Table 1. Lines in the SPIRE spectra of IRAS 05280−6910.

Line Name	ν_0 (GHz)	ν (GHz)	v (km s^{-1})	Int. Flux ($\times 10^{-18}$ W m^{-2})
SLW (the SPIRE long wavelength band)				
CO J=6–5	691.47	691.06	181 ± 130	1.4 ± 0.7
CO J=7–6	806.65	806.23	155 ± 63	2.5 ± 0.7
p-H2O(ν_2=1,3_{12}–2_{21})	902.61	902.22	129 ± 118	1.3 ± 0.7
p-H2O(9_{28}–8_{35})	906.21	905.41	262 ± 94	1.6 ± 0.7
CO J=8–7	921.80	921.05	244 ± 44	3.2 ± 0.7
p-H_2O (2_{02}–1_{11})	987.93	987.19	224 ± 22	6.0 ± 0.7
SSW (the SPIRE short wavelength band)				
p-H_2O (2_{02}–1_{11})	987.93	987.14	240 ± 40	3.6 ± 0.7
CO J=9–8	1036.91	1036.09	238 ± 54	2.6 ± 0.7
o-H_2O (3_{12}–3_{03})	1097.36	1096.31	288 ± 50	2.6 ± 0.7
p-H_2O (1_{11}–0_{00})	1113.34	1112.05	349 ± 51	2.5 ± 0.7
CO J=10–9	1151.99	1150.95	271 ± 75	4.6 ± 1.4
o-H_2O (3_{12}–2_{21})	1153.13	1152.09	271 ± 46	7.4 ± 1.5
o-H_2O (6_{34}–5_{41})	1158.32	1157.23	282 ± 59	2.2 ± 0.8
o-H_2O(3_{21}–3_{12})	1162.91	1161.85	274 ± 22	5.9 ± 0.8
p-H_2O(4_{22}–4_{13})	1207.64	1206.74	223 ± 15	8.2 ± 0.7
o-H_2O(ν_2=1, 3_{12}–3_{03})	1214.66	1213.36	322 ± 50	2.4 ± 0.7
p-H_2O (2_{20}–2_{11})	1228.79	1227.67	274 ± 30	4.0 ± 0.7
CO J=11–10	1267.01	1265.89	266 ± 18	6.4 ± 0.7
o-H_2O (7_{43}–6_{52})	1278.27	1277.03	289 ± 40	2.9 ± 0.7
o-H_2O (8_{27}–7_{34})	1296.41	1295.98	101 ± 115	1.0 ± 0.7
o-H_2O (6_{25}–5_{32})	1322.07	1320.60	332 ± 27	4.2 ± 0.7
CO J=12–11	1382.00	1380.75	270 ± 14	7.5 ± 0.7
o-H_2O (5_{23}–5_{14})	1410.65	1409.34	277 ± 18	5.9 ± 0.7
CO J=13–12	1496.93	1495.66	253 ± 13	7.3 ± 0.7

Notes. ν_0: vacuum frequency, ν: measured frequency, v: velocity shift

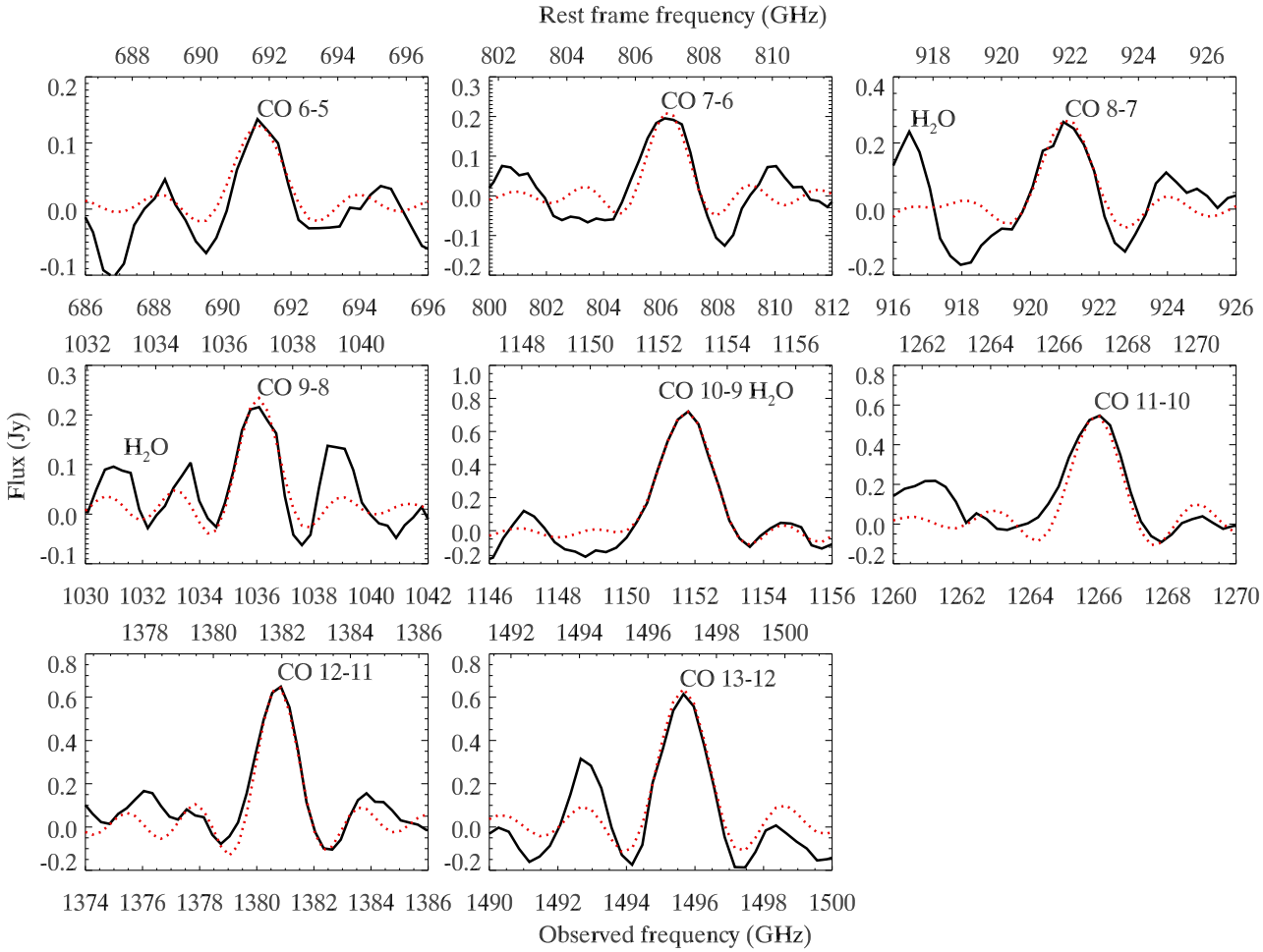

Figure 2. The SPIRE FTS unapodized spectra of the CO lines (continuous lines) of IRAS 05280-6910, with instrumental model line profiles (red dotted lines; Naylor et al. 2014).

all three lines from IRAS 05280−6910 while only CO $J = 15$–14 was detected from WOH G64. The lines observed by PACS were fitted by Gaussians with a quadratic underlying continuum, allowing the line strength, line centre, line width, and coefficients of the quadratic continuum all to be free parameters. These Gaussians were fit to the lines plus surrounding long- and short-wavelength continuum, except that the wings of the 92 μm H_2O line of IRAS 05280−6910 were removed from the fitting process, in order for the Gaussian to converge to a sensible fit. The Gaussian fittings are plotted with red dotted lines in the figure, and the line intensities were estimated by integrating the Gaussian profiles. The measured line intensities are summarized in Table 2.

4 ANALYSIS

4.1 Spectral line energy distributions

In order to examine the excitation temperature and column density of CO, spectral line energy distributions (SLEDs) were used. Fig. 4 shows the SLED of IRAS 05280−6910. The single CO line measurement of WOH G64 has also been plotted. The figure also shows *Herschel* measurements of SLEDs of the Galactic RSG VY CMa and the Galactic AGB star W Hya (Matsuura et al. 2014; Khouri et al. 2014b). The SLEDs of VY CMa and W Hya were scaled to the LMC distance, by adopting their stellar distances of 1.14 kpc and 78 pc, respectively (Knapp et al. 2003; Choi et al. 2008).

4.2 Non-LTE line radiative transfer modelling

In order to derive physical parameters from CO line intensities, a non-local thermodynamic equilibrium (non-LTE) line radiative transfer code was used to fit the SLEDs. As only IRAS 05280−6910 has multiple CO transitions detected, we focus our modelling effort on this RSG.

The first step was to construct a dust radiative transfer model to fit the SED. This step provided some essential parameters for the CO modelling, such as dust temperature structure, which has an effect on the heating balance between dust and gas collisions. Modelling the SED with DUSTY provides the inner radius, the dust radial density and the temperature distribution of the dust envelope. These parameters were also converted into a dust mass-loss rate, and, hence, gas mass-loss rate, with an assumption of the gas-to-dust ratio. Boyer et al. (2010) already presented modelling of the SED of IRAS 05280−6910 using 2-DUST code (Ueta & Meixner 2003). We started by reproducing the 2-DUST results with DUSTY (Ivezic & Elitzur 1997), as the DUSTY model is one of our default input models to CO modelling. We used the IR flux measurements of IRAS 05280−6910 collected by Boyer et al. (2010), including

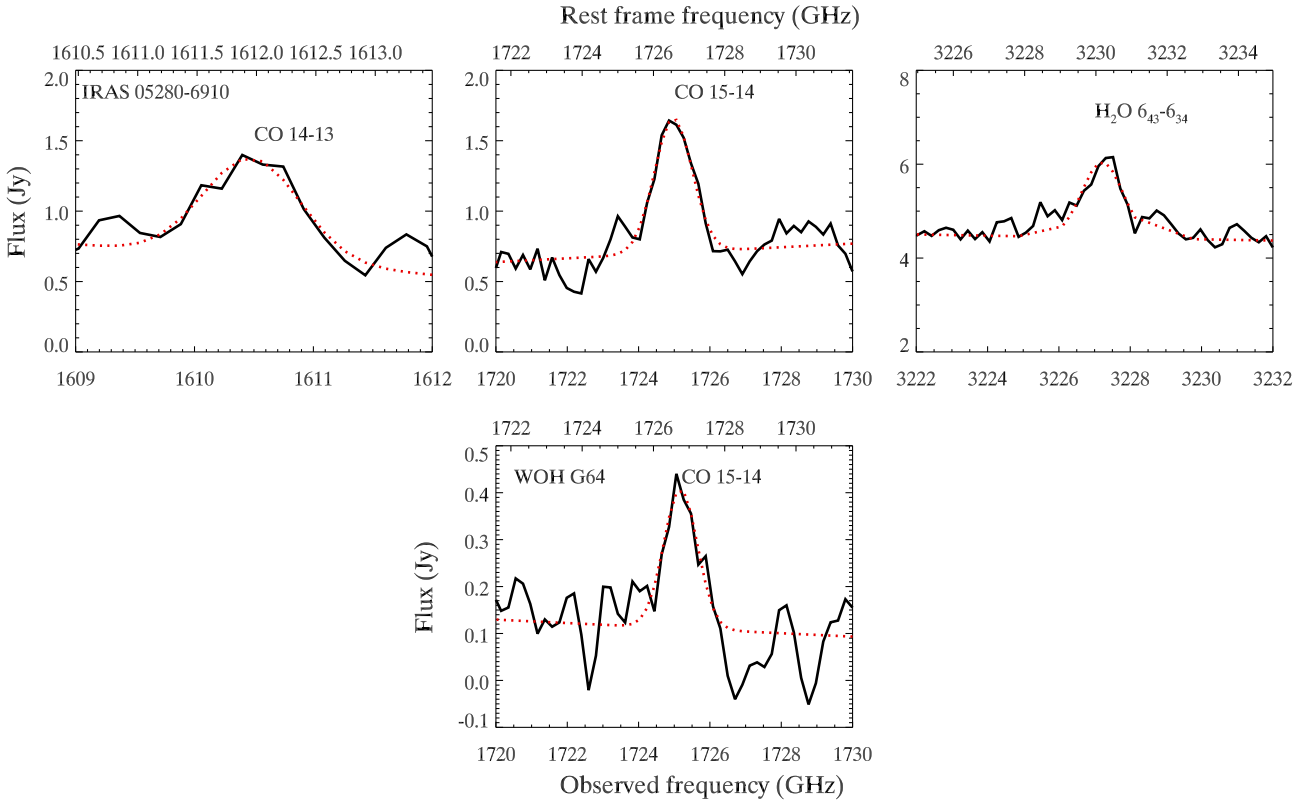

Figure 3. The PACS spectra of IRAS 05280-6910 (top) and WOH G64 (bottom). The red dotted lines show weighted Gaussians fitted to the measured lines.

Table 2. PACS measurements of CO and H_2O in IRAS 05280−6910 and WOH G64 spectra.

Line Name	ν_0 (GHz)	ν (GHz)	v (km s^{-1})	Int. Flux (10^{-18} W m^{-2})
IRAS 05280−6910				
CO J=14–13	1611.79	1610.50	242 ± 12	7.4 ± 1.7
CO J=15–14	1726.60	1724.99	280 ± 6	12.7 ± 1.2
H_2O 6_{43}–6_{34}	3230.14	3227.24	269 ± 4	23.0 ± 2.8
WOH G64				
CO J=15–14	1726.60	1725.19	245 ± 11	3.5 ± 0.7

Notes. ν_0: vacuum frequency, ν: measured frequency, v: velocity shift.

3–24 μm photometric data from *Spitzer* Magellanic Survey, SAGE (Meixner et al. 2006), the measurements of *Herschel* Magellanic Survey, HERITAGE (Meixner et al. 2013) covering 100–500 μm, and at 5–35 μm a *Spitzer* IRS spectrum (SAGE-spec; Kemper et al. 2010). We used *Ks*-band magnitudes from the VISTA Magellanic Cloud survey (VMC; Cioni et al. 2011), prior to their public release of the magnitude of this star. The PSF fitting resulted in a magnitude of 12.604±0.080 in the *Ks*-band. It was converted to a Vega-system magnitude following the procedure described in Rubele et al. (2015), then converted to a flux in Jy. The source was not detected in the VMC z and J-bands.

An effective temperature of 3000 K was adopted for IRAS 05280−6910 (Boyer et al. 2010). This is similar to the estimated temperature of WOH G64 and VY CMa which have similar mass-loss rates of $\sim 10^{-4}$ $M_\odot$ yr^{-1}. The effective temperature of VY CMa has been estimated to be in the range from 2700 K

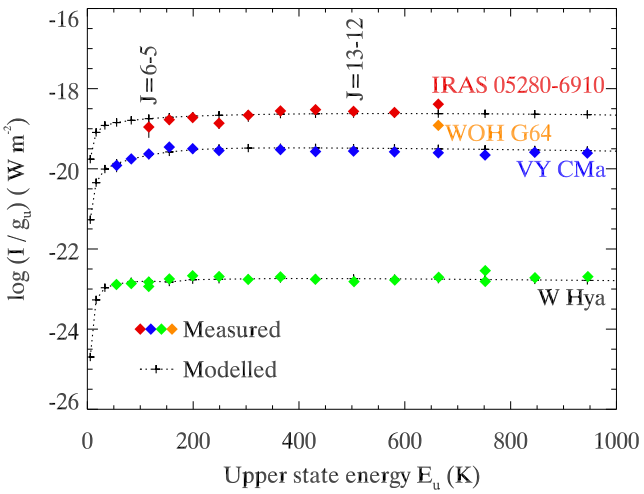

Figure 4. The spectral line energy distribution (SLED) for IRAS 05280−6910, VY CMa and W Hya (diamonds), with a single CO line measurement for WOH G64. The SLEDs of VY CMa and W Hya were scaled to the LMC distance, by adopting their stellar distances of 1.14 kpc and 78 pc, respectively (Knapp et al. 2003; Choi et al. 2008). The non-LTE model fits are displayed with dotted lines.

(Monnier et al. 2004) to 3650 K (Massey, Levesque & Plez 2006). Elias et al. (1986) estimated a spectral type of M7.5 for WOH G64, corresponding to an effective temperature lower than 3450 K (=M5; Levesque et al. 2005), while Ohnaka et al. (2008) suggested to be 3200–3400 K. Davies et al. (2013) argued that the effective temperature of RSGs should be higher than previously thought by ∼500 K. Our experimental modelling with the effective temperature

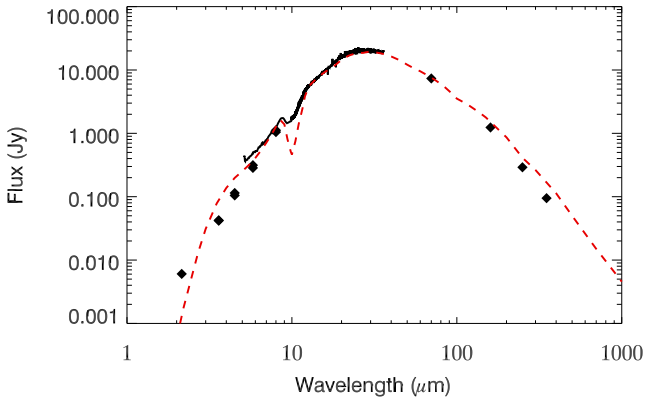

Figure 5. The spectral energy distribution of IRAS 05280−6910. The measured infrared fluxes are from the sources described in the text. The red dashed line shows the dust radiative transfer model fit to the SED.

increased to 3500 K resulted in a negligible (<5 per cent) increase in CO line intensities. We therefore adopted the 3000 K effective temperature from Boyer et al. (2010) but little difference in the CO modelling results for an effective temperature of 3500 K.

Our DUSTY fitted results for IRAS 05280−6910 are displayed in Fig. 5. The overall shape of the SED was fitted with silicate dust emission. As found by Boyer et al. (2010), our modelling produced silicate absorption stronger than that observed. This could be due to the outflow being slightly asymmetric, as recently found for the Galactic RSG VY CMa (O'Gorman et al. 2015). However, currently we do not have any information about asymmetries for IRAS 05280−6910, so we adopted symmetric modelling. Alternatively, Boyer et al. (2010) suggested a potential contribution of silicate emission from a nearby RSG (WOG G347) on to the *Spitzer* IRS slit, but not visible at longer wavelengths. Our DUSTY parameters are summarized in Table 3, which are consistent with those obtained from Boyer et al. (2010)'s 2-DUST modelling. We evaluated the DUSTY input parameters with a χ^2-analysis. We found that $T_{\rm dust}$ and τ are coupled parameters, and the uncertainty of the dust temperature is ±50 K, and that of the optical depth at 0.55 μm ($\log\tau_{0.55}$) is ±0.1, with increasing dust temperature requiring higher dust optical depth. We used dust optical constants for amorphous silicates (Ossenkopf, Henning & Mathis 1992), and the MRN grain size distribution with an index of 3.5, and grain size of 0.005–1 μm (Mathis, Rumpl & Nordsieck 1977). Assuming a gas-to-dust ratio of 500, which is expected from the abundance of refractory elements in the LMC interstellar medium (ISM) (Gordon, Roman-Duval & Bot 2014), the SED modelling resulted in a gas-mass loss rate of 3×10^{-4} $M_\odot$ yr^{-1}. That carries 30 per cent uncertainty, according to the DUSTY manual.[1]

The second part of our modelling was to reproduce the CO rotational lines using the non-LTE line radiative transfer calculation and level population code, SMMOL (Rawlings & Yates 2001). The SMMOL code adopts the accelerated lambda integration scheme (Scharmer & Carlsson 1985; Rybicki & Hummer 1991) with an ability to solve the radiative transfer problems in optically thin and thick circumstellar envelopes. Solving level populations requires cross-sections for molecular collision, and we adopted the CO–H_2 cross-sections calculated by Yang et al. (2010), with molecular data from Müller et al. (2005). The code has been used for modelling the SLEDs of CO from $J = 4$–3 to 22–21, as well as for H_2O masers in the Galactic RSG, VY CMa (Matsuura et al. 2014).

[1] www.pa.uky.edu/~moshe/dusty/

Table 3. Model parameters for IRAS 05280−6910.

DUSTY	
T_* (K)	3000
Dust	Silicate (Ossenkopf & Henning 1994)
$T_{\rm dust}$ (K)	350±50
$\dot{M}_{\rm g}$($M_\odot$ yr^{-1})	$3 \pm 1 \times 10^{-4}$
gas-to-dust	500 (Gordon et al. 2014)
log $\tau_{0.55}$	0.56±0.1
SMMOL	
R_* (cm)	1.21×10^{14} (calculated from the luminosity and T_*)
$R_{\rm in,molecules}$ (cm)	1.21×10^{14} ($= R_*$)
$R_{\rm in,dust}$ (cm)	2.07×10^{16} (adopted from the DUSTY output)
$R_{\rm out}$ (cm)	2.07×10^{18}
β : $\rho \propto (r/R_{\rm inner})^{-\beta}$	2
α: $T \propto (r/R_{\rm inner})^{-\alpha}$	0.25 ($@R < R_{\rm in,dust}$)
	0.6±0.2 ($@R > R_{\rm in,dust}$)
$v_{\rm turb}$ (km s^{-1})	1.0
number of CO/H_2	2.7×10^{-4}
log $\tau_{0.55}$	1.56 (adopted from the DUSTY output)
$\dot{M}_{\rm g}$($M_\odot$ yr^{-1})	3×10^{-4} (consistent to the DUSTY output)
Gas-to-dust	500 (Gordon et al. 2014)
$v_{\rm term}$ (km s^{-1})	17 (Marshall et al. 2004)
$v_{\rm in}$ (km s^{-1})	4.0
$R_{\rm in,velocity}$ (cm)	1.283×10^{15}
γ (velocity gradient)	0.2
$T_{\rm sub}$ (K)	20

Notes. T: temperature, R: radius, $\tau_{0.55}$: optical depth at 0.55 μm, $\dot{M}_{\rm g}$: gas mass-loss rate, β: density law index, $(r/R_{\rm inner})^{-\beta}$, α: kinetic temperature law index, $(r/R_{\rm inner})^{-\alpha}$, $v_{\rm term}$: wind terminal velocity, $v_{\rm in}$: wind inner velocity, $R_{\rm in,velocity}$: radius where the wind velocity of $v_{\rm in}$ starts, γ: velocity law index, $v(r) = v_{\rm inner} + (v_\infty - v_{\rm inner})\,(1 - R_{\rm inner,dust}/r)^\gamma$, for $r \geq R_{\rm inner,dust}$, and $T_{\rm sub}$: sublimation temperature of CO.

The majority of the SMMOL input parameters for IRAS 05280−6910 were constrained from SED modelling work prior to the CO modelling. Integrating over the SED provided luminosity of 2.2×10^5 $L_\odot$ (Boyer et al. 2010). As discussed above, an effective temperature of 3000 K was adopted for IRAS 05280−6910 (Boyer et al. 2010). These two parameters yielded a radius for the star ($R_{\rm star}$) of 1.21×10^{14} cm ($= 1738$ $R_\odot$). The DUSTY model provided the inner radius, radial density and temperature structure of the dust envelope, as well as the optical depth ($\tau_{0.55}$). The parameters used for the IRAS 05280−6910 non-LTE modelling are listed in Table 3. Another important parameter is the gas terminal velocity, which was adopted to be 17 km s^{-1}, based on OH maser measurements (Marshall et al. 2004). The majority of our input parameters were already well constrained from previous studies.

The CO–H_2 abundance ratio is affected by the metallicity. A chemical model for the oxygen-rich AGB stars shows that essentially all available C atoms are locked up to CO (Willacy & Millar 1997), so that the C abundance with respect to H_2 gives the CO abundance. Scaling with the solar-abundance values for carbon with respect to hydrogen (8.43; Asplund et al. 2009), and taking [Z/H] $= -0.3$ for the LMC, the estimated CO–H_2 abundance is 2.7×10^{-4}. Overall, the model predicts that the high-J CO line intensities scaled with the CO abundance i.e. a metallicity effect is found for the high-J CO line intensities. The adopted CO/H_2 abundance ratio was based on the C and O abundances of the Sun, scaled to the LMC metallicity, however, C and O abundances of high-mass

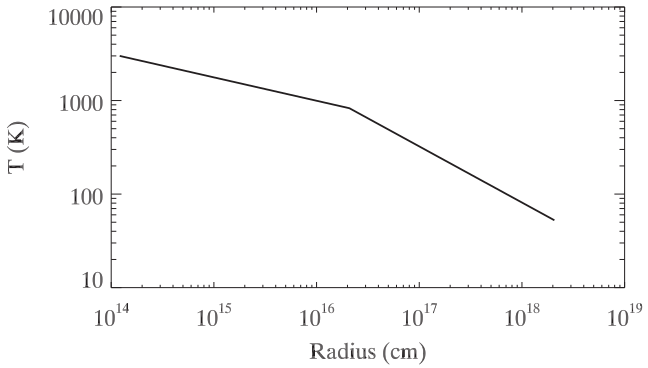

Figure 6. The temperature structure used for SMMOL modelling.

stars can be potentially modified due to nuclear synthesis (Meynet et al. 2015). The current work ignores this effect.

Three parameters were adopted from the VY CMa modelling (Matsuura et al. 2014): the temperature and velocity structure gradient indices, and the turbulent velocity. A turbulent velocity of 1 km s^{-1} was adopted (Decin et al. 2006; Matsuura et al. 2014). The kinetic temperature gradient index α, where $T_{\rm kin} \propto (r/R_{\rm inner})^{-\alpha}$, has not yet been determined for circumstellar envelopes at low metallicity. The balance between cooling and heating processes determines the temperature gradient. Two major cooling processes are adiabatic cooling and H_2O line emission (Decin et al. 2006). The H_2O abundance has a metallicity dependence, as it is limited by the available oxygen abundance. The H_2O cooling is expected to be less efficient at low metallicity. On the other hand, key gas heating processes in the circumstellar envelope are associated with collisions with dust grains (Decin et al. 2006). At low metallicity, the dust-to-gas ratio is small; hence the heating rate is expected to be low, too. Depending on the balance between these heating and cooling processes, the temperature gradient can change slightly at low metallicity. However, we found that changing α at $R > R_{\rm dust}$ from 0.5 to 0.6 made less than a few per cent difference to the predicted CO line intensities. Such a small difference in the gas gradient in the circumstellar envelope is not crucial for CO modelling. We adopted of 0.6, the α value found for VY CMa (Matsuura et al. 2014), and the adopted temperature structure is plotted in Fig. 6. Similarly, we examined α at $R < R_{\rm dust}$, by changing the value of VY CMa (0.15) to 2.5. There was negligible difference in the predicted CO line intensities. The value of $\alpha = 0.25$ was used at $R < R_{\rm dust}$.

The velocity structure parameter, γ describes the velocity structure of the wind acceleration region. However, the CO emitting region (approximately $r > 100R_*$) is outside of the wind accelerating region, so γ is not important for the CO modelling. Experimentally, when we changed γ up to 5, the obtained CO line intensities remained unchanged, because the velocity structure at $r > 100R_*$ does not change. Constraining γ requires measurements of the velocity structure in the inner region. That has been estimated for Galactic RSGs (Decin et al. 2010), suggesting γ to be less than 1. We adopted $\gamma = 0.2$, following our modelling of VY CMa (Matsuura et al. 2014).

A density (ρ) law index $\beta = 2$, where $\rho \propto (r/R_{\rm inner})^{-\beta}$, is adopted for the gas with a constant expansion velocity. Although this is not the case near the velocity accelerating region, because this inner part does not affect the observed CO line intensities, it is not a major issue.

The outer radius ($R_{\rm out}$) was chosen to be large enough that predicted CO line intensities were unaffected by $R_{\rm out}$. As $J = 6$–5 and higher CO transitions have their line forming regions much closer to the central star than low-J CO lines (1–0 or 2–1; Khouri et al. 2014b), these high-J line intensities are less sensitive to the choice of $R_{\rm out}$. The $R_{\rm out}$ is the value corresponding to the dissociation radius of CO due to ISM UV radiation. In the LMC, a higher ISM UV radiation field is expected than for the Galactic ISM, due to low dust extinction. Hence, UV photons might penetrate further into the circumstellar envelope, dissociating CO at smaller radii in the LMC RSGs than for the Galactic counterparts McDonald & Zijlstra (2014). Fortunately, such a low metallicity effect would not be important for the high-J CO line intensities.

In summary, although there are several parameters in SMMOL modelling, key input parameters are the gas mass-loss rate and CO/H_2 abundance ratio, which determine overall height of CO line intensities, and temperature index α that manipulates the tilt of the CO SLED.

4.3 Modelling results

Our CO modelling results for IRAS 05280−6910 are displayed in Fig. 4. The measured CO line intensities are well fitted, particularly $J = 11$–10 to 15–14. By modelling CO emission lines, CO mass-loss rate is determined, which is used to estimate gas mass-loss rate, assuming CO/H_2 abundance ratio. We found that the estimated mass-loss rates of IRAS 05280−6910 from the dust modelling to the SED and from modelling to CO emission are consistent.

The metallicity affects both the CO/H_2 abundance ratio and dust-to-gas ratio in a similar manner. Both ratios are essentially scale with the metallicity, represented by [Fe/H]. The gas-to-dust ratio accounts for the available refractory elemental abundance. Assuming that silicates are the major dust component in oxygen-rich circumstellar environment, such as the RSGs, and that the silicon abundance limits the total dust mass, the estimated gas-to-dust mass ratio would be about 450. We adopted Gordon et al.'s (2014) estimate of 500, which is consistent with the above estimate. Similarly, the CO-H_2 abundance ratio accounts for the number of carbon atoms, and this parameter also scale to [Fe/H]. Essentially, the values of 'dust-to-CO ratio' are the same both with solar and LMC metallicities.

5 DISCUSSIONS

5.1 CO emission

With the *Herschel* SPIRE and PACS spectrometers, we have detected CO emission from IRAS 05280−6910 and WOH G64, with multiple CO detections from IRAS 05280−6910. We modelled the IRAS 05280−6910 SED with a dust radiative transfer code, constraining the mass-loss rate and the structure of the circumstellar envelope. These dust model parameters were used to further model the CO rotational lines, resulting in good fits to the lines.

Although the LMC has approximately half the solar metallicity (Cole et al. 2005), there is no obvious metallicity effect on CO line intensities between Galactic and LMC RSGs. Fig. 4 shows the measured and modelled CO SLEDs of the Galactic RSG VY CMa (Matsuura et al. 2014) and the Galactic AGB star W Hya (Khouri et al. 2014b). The overall shapes of the CO SLEDs are alike for all three stars, showing a sharp increase of CO at $J = 1$–0 to 4–3, and flattening out at higher J. No clear evidence of reduced CO intensity at lower metallicity is found in our limited sample.

Lagadec et al. (2010) reported the detection of CO rotational lines from carbon-rich AGB stars, which are likely to be linked

Table 4. Luminosities and mass-loss rate of AGB stars and red-supergiants investigated via *Herschel* CO SLEDs.

Name	Luminosity ($L_\odot$)	Mass-loss rate ($M_\odot$ yr^{-1})	v_{exp} (km s^{-1})	References
IRAS 05280−6910	2.2×10^5	$\sim 10^{-3}$ (IR) 3×10^{-4} (IR+CO)	17	Boyer et al. (2010), Marshall et al. (2004) This work
WOH G64	$2.8 \pm 0.4 \times 10^5$	2.3×10^{-5} (IR)	24	Ohnaka et al. (2008), van Loon et al. (1999), Marshall et al. (2004)
VY CMa	$\sim 5 \times 10^5$	2×10^{-4} (CO)	32	Smith et al. (2001), Choi et al. (2008), De Beck et al. (2010), Richards, Yates & Cohen (1998)
W Hya	5400	1.5×10^{-7} (CO)	3–6	Khouri et al. (2014b), Khouri et al. (2014a), Loup et al. (1993)

with the Sagittarius Dwarf Spheroidal Galaxy (Sgr dSph) stream. The Sgr dSph has a metallicity of [Fe/H] ~ -1.1 (van den Bergh 2000). They concluded that there is no reduction in the gas mass-loss rates from carbon-rich AGB stars at this low metallicity. In the case of carbon-rich AGB stars, the main composition of the dust is carbon, and carbon has been synthesized and dredged up to the surface (e.g. Karakas et al. 2009), and radiation pressure on carbonaceous dust grains can trigger mass loss. Hence, it is not totally surprising that no correlation was found between mass-loss rates and metallicities for carbon-rich AGB stars.

By contrast, the dust mass in oxygen-rich AGB stars and RSGs is expected to be restricted by the number of silicon atoms. The silicon abundance is intrinsic to the star, i.e. limited by the silicon atoms incorporated the stars at the time of stellar formation, although silicon might be synthesized during the very last few hundred years of the RSG phase (Weaver & Woosley 1980). Reduced mass-loss rates are predicted at low metallicities for oxygen-rich AGB stars and RSGs (Bowen & Willson 1991). Therefore, it is more surprising to see no metallicity effects on the mass-loss rates for RSGs than it is for carbon-rich AGB stars.

Instead, we found that the CO line intensities and the mass-loss rate largely depend on the luminosity/luminosity class. The AGB star, W Hya, which has about a factor of 50–100 lower luminosity than VY CMa and IRAS 05280−6910 (Table 4), has about a factor of 1000 weaker CO ladder than the other two. The luminosity appears to play the dominant role in CO line intensities and mass-loss rates.

5.2 Mass-loss rates and luminosities at low metallicity

We found from our small sample that CO line intensities and gas mass-loss rates tend to increase with higher luminosities. In order to further investigate the impact of luminosity, as well as metallicity, on the mass-loss rate of evolved stars, we compare here the mass-loss rates of these stars with that of a larger sample.

The sample of Galactic stars was taken from De Beck et al. (2010) with 47 AGB stars and RSGs. We uses this sample because they used both IR SED and CO lines in order to derive the mass-loss rates. The Luminosities of Galactic stars were estimated from a period–luminosity relation. For LMC stars, the sample of the 172 oxygen-rich stars from Groenewegen et al. (2009) was used, where the mass-loss rate estimates were obtained by IR SED modelling. They assumed an expansion velocity of 10 km s^{-1} and a gas-to-dust ratio of 200 for all AGB stars and RSGs. These assumptions can provide a factor of a few uncertainty in their mass-loss rates, but do not have a critical impact on our systematic analysis.

Fig. 7 shows the mass-loss rate versus luminosity relation for the LMC and Galactic evolved stars. The Galactic evolved stars follow

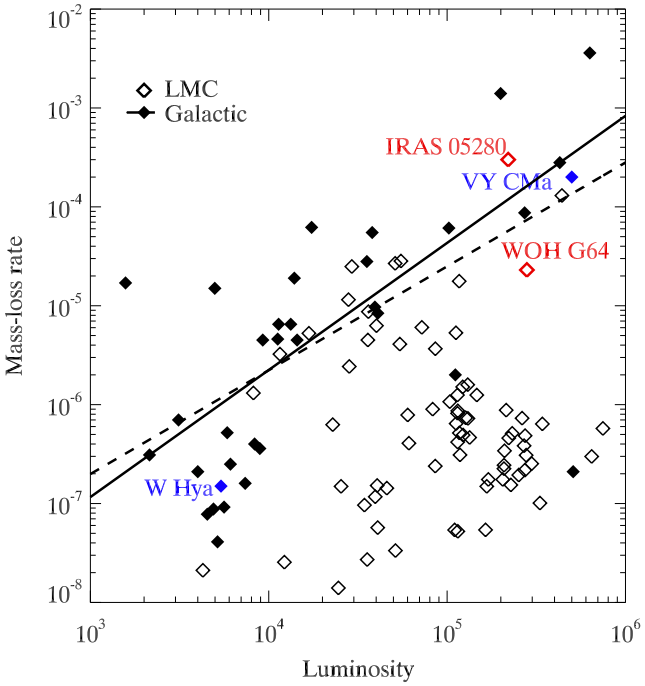

Figure 7. The mass-loss rate ($M_\odot$ yr^{-1}) versus luminosity ($L_\odot$) for oxygen-rich AGB stars and red supergiants in the Galaxy and the LMC. The Galactic data are taken from De Beck et al. (2010), and the LMC data are from Groenewegen et al. (2009). The solid line shows the mass-loss versus luminosity relation fitted to Galactic sample, and the dashed line shows the mass-loss versus luminosity relation for T_{eff} =3500 K stars in the LMC (van Loon et al. 2005a).

an increasing trend of mass-loss rate with higher luminosity. This trend was fitted with a 'robust' least deviation method by removing outliners (Press et al. 1992), yielding

$$\log(\dot{M}_g) = -10.79 + 1.29 \log(L_*). \quad (1)$$

The fitted line is indicated in Fig. 7. Both VY CMa and W Hya, which have *Herschel* CO SLEDs, follow this line.

In contrast, the LMC sample scatters across Fig. 7. Although the majority of LMC stars are placed lower than the line fitted to the Galactic objects, two stars we studied (IRAS 05280−6910 and WOH G64) follow this Galactic trend. Further, these two stars have among the highest mass-loss rates in the LMC. Actually, the Galactic line approximately captures the upper range of mass-loss rates at a given luminosity amongst the LMC sample.

The fitted mass-loss rate versus luminosity relation for Galactic stars is similar to that found by van Loon et al. (2005a) for LMC stars. Their analysis of 23 stars in the LMC produced the relation

plotted as a dashed line in Fig. 7. The line plotted in the figure is for $T_{\rm eff} = 3500$ K. For a $T_{\rm eff} = 3000$ K star, the mass-loss rate is a factor of 2.6 higher at a given luminosity, which is small compared with scatter in the sample. van Loon et al. (2005a)'s LMC fit follows a similar trend to that found here for the Galactic stars, but this fit indicates only the upper range of mass-loss rate at a given luminosity for the larger LMC sample (Groenewegen et al. 2009).

The question is why LMC evolved stars show a much larger scatter of mass-loss rate at a given luminosity than Galactic objects. We argue that this is due to biases in the samples. Both the LMC and Galactic stars could have a large scatter, but Galactic sample tend to have picked up bright CO objects. De Beck et al. (2010)'s study was optimized for verifying models for circumstellar envelopes with firm CO detections, rather than optimising for a volume-limited CO line survey. The majority of the CO sample of De Beck et al. (2010) were taken at JCMT or APEX (Kemper et al. 2003). As Kemper et al. (2003) selected bright samples from Loup et al. (1993)'s CO catalogue, it is possible that mass-loss stars with weak CO lines have not been included in their target list. Hence, the Galactic sample could appear at an upper end of the mass loss versus luminosity relation.

As there are no systematic LMC studies of CO emission beyond our two objects, studies of mass-loss rates in LMC evolved stars have relied on IR SEDs. The LMC sample here is from Groenewegen et al. (2009), who assembled *Spitzer* IRS spectra from six different observing programmes. The targets of these programmes were selected mostly from the 2MASS near-IR survey (Skrutskie et al. 2006), or from a combination of 2MASS and MSX (Egan, Van Dyk & Price 2001), with the exception of a few objects with optical light curves (Sloan et al. 2008). The near-IR and optical surveys are efficient for detecting evolved stars with relatively low mass-loss rates, but inefficient of detecting dust-embedded AGB stars and RSGs. For example, IRAS 05280−6910 does not have a 2MASS counterpart. The surveys detected a range of stars with mass-loss rate below $>10^{-5}$ M$_\odot$ yr^{-1} but only a few stars with $L > 10^5$ L$_\odot$, and mass-loss rate $>10^{-6}$ M$_\odot$ yr^{-1} was found in Groenewegen et al.'s (2009) sample. We argue that due to the selection methods, Groenewegen et al.'s (2009) LMC sample does not contain RSGs with high optical depth dust shells.

The reason for the wide scatter in mass-loss rate and luminosity could be very interesting. One of the possibilities is that the AGB stars that experience the third dredge up have an enhanced mass-loss rate (e.g. Vassiliadis & Wood 1993), reaching the upper range of the mass-loss rate and luminosity relation.

Mauron & Josselin (2011) reported a metallicity dependence for IR-SED mass-loss rates, using RSGs in the Large and Small Magellanic Clouds (Bonanos et al. 2010). The mass-loss rates would be scaled by the metallicity $(Z/Z_\odot)^{0.7}$. Their definition of mass-loss rate was based on $K_{\rm s} - [12]$, a good indicator of dust mass-loss rate. Such a metallicity dependence was not detected from a comparison on three *Herschel* CO SLEDs nor from a comparison between the results by Groenewegen et al. (2009) and De Beck et al. (2010). Detecting metallicity effects could require a much larger CO sample.

5.3 The contribution of high mass-loss RSGs to the global dust and gas source in the LMC

Evolved stars, both AGB stars and RSGs are considered to be important sources of dust and gas of the ISM (Gehrz 1989; Dwek 1998; Tielens 2010) After *Spitzer*'s launch, IR colours and magnitudes were used to estimate individual mass-loss rates of evolved stars, and global gas and dust inputs from evolved stars into the ISM estimated for studied in the Large and Small Magellanic Clouds (e.g. Matsuura et al. 2009; Srinivasan et al. 2009). These studies found that a few high mass-loss rate stars dominate the global inputs of dust and gas from evolved stars. The mass-loss rate of IRAS 05280−6910 is at the high-end range even amongst RSGs, and it must be an important source of gas and dust.

Matsuura, Woods & Owen (2013) used 2MASS $K_{\rm s}$ magnitudes for object classifications for high mass-loss rate RSGs, but IRAS 05280−6910 does not have 2MASS measurements. Similarly, Boyer et al. (2012) and Riebel et al. (2012) also used 2MASS photometry for their target selection. So IRAS 05280−6910 was excluded from the accounting of the global gas and dust inputs into the ISM in these two studies.

High mass-loss rate stars, such as IRAS 05280−6910 can contribute a significant fraction of the total dust and gas input from evolved stars into the ISM. Matsuura et al. (2013) estimated the total gas input rate from AGB stars and RSGs to be 1.5×10^{-2} M$_\odot$ yr^{-1}. With a gas mass-loss rate of 2×10^{-4} M$_\odot$ yr^{-1}, IRAS 05280−6910 contribute 2 per cent of the total gas input from LMC evolved stars. Boyer et al. (2012) estimated the total 'dust' input rate from AGB stars and RSGs to be to be 1.4×10^{-5} M$_\odot$ yr^{-1}. The dust mass-loss rate of IRAS 05280−6910 is estimated to be 5×10^{-7} M$_\odot$ yr^{-1}, contributing about 4 per cent of the total dust input from evolved stars. If reasonable fractions of dust grains from RSGs may survive subsequent SN explosions, high mass-loss rate RSGs can account for a substantial fraction of input to the global gas and dust budget of the LMC.

The dust contributions from RSGs to the ISM dust are subject to subsequent dust destruction by SN shock waves, and that is largely uncertain. Theoretical estimated values of the dust survival rate depend on models, from 20 to 62 per cent (Silvia, Smith & Shull 2010) to nearly 100 per cent (Nozawa et al. 2010; Bocchio, Jones & Slavin 2014). Turning to examples of nearby supernovae remnants (SNRs) with large dust mass detected (e.g. Barlow et al. 2010; Gomez, Krause & Barlow 2012; Matsuura et al. 2015), both Cassiopeia A and SN 1987A show the presence of reverse shocks (Gotthelf et al. 2001; France et al. 2010), and dust was detected from the unshocked regions (Barlow et al. 2010; Indebetouw et al. 2014). In contrast, the dominant energy in the Crab nebula is currently from its pulsar wind nebula. In the older SNR, the Cygnus Loop, an enhanced C abundance in shocked region suggests the destruction of carbonaceous dust Raymond et al. (2013), but this could be swept-up ISM dust. Temim et al. (2015) and Lakićević et al. (2015) studied SNRs in the LMCs, and estimated that dust overall destroyed by SNe. Lakićević et al. (2015) found that the temperature of SNR dust emission to be higher than that of ISM dust, which affect their dust mass analysis. In the optically thin case, the thermal emission from warmer SN dust can dominate the total emission, hiding weaker emission from colder ISM dust. This effect distort the measured ISM dust mass towards the SNRs rather than the ISM dust mass being actually lower towards the SNRs due to SN shocks destroying surrounding ISM dust grains. A challenge remains in measuring dust mass destroyed by SNe.

6 SUMMARY

We have detected far-IR and sub-millimetre CO and H_2O lines from two RSGs in the LMC. These are the first detections of these lines in LMC evolved stars.

Modelling with radiative transfer codes of the dust and line emission resulted in good fits to the IR-SED and CO transitions of

IRAS 05280−6910. A mass-loss rate of 3×10^{-4} $M_\odot$ yr^{-1} was obtained, and a value is at the high end of mass-loss rates found for RSGs. A gas-to-dust ratio of 500 and a CO/H_2 abundance of 2.7×10^{-4} were adopted for the modelling. The gas-to-dust ratio was adopted from the value estimated for the LMC ISM, but is consistent with the solar neighbourhood value scaled by the LMC metallicity. The CO/H_2 abundance was adopted from the Galactic value scaled by the LMC metallicity. Our good modelling results support CO/dust ratio appears to be constant in the Galactic and LMC RSGs.

There is a general increasing trend of mass-loss rate with higher luminosity. The LMC RSGs with CO detections appear at the an upper range of mass-loss rate at a given luminosity. Among CO-detected AGB stars and RSGs, there is no obvious metallicity effect found between Galactic and LMC stars and object-to-object variation overwhelms the metallicity dependence, if any.

ACKNOWLEDGEMENTS

We would like to thank Dr S. Srinivasan for useful inputs on χ^2 analysis on DUSTY fitting. MM is supported by the STFC Ernest Rutherford fellowship. M. Meixner and BS acknowledge funding from the NASA Astrophysics Data Analysis Program grant NNX13AD54G and from the NASA/JPL grant NNN12AA01C. PACS has been developed by a consortium of institutes led by MPE (Germany) and including UVIE (Austria); KU Leuven, CSL, IMEC (Belgium); CEA, LAM (France); MPIA (Germany); INAF-IFSI/OAA/OAP/OAT, LENS, SISSA (Italy); IAC (Spain). This development has been supported by the funding agencies BMVIT (Austria), ESA-PRODEX (Belgium), CEA/CNES (France), DLR (Germany), ASI/INAF (Italy), and CICYT/MCYT (Spain). SPIRE has been developed by a consortium of institutes led by Cardiff University (UK) and including Univ. Lethbridge (Canada); NAOC (China); CEA, LAM (France); IFSI, Univ. Padua (Italy); IAC (Spain); Stockholm Observatory (Sweden); Imperial College London, RAL, UCL-MSSL, UKATC, Univ. Sussex (UK); and Caltech, JPL, NHSC, Univ. Colorado (USA). This development has been supported by national funding agencies: CSA (Canada); NAOC (China); CEA, CNES, CNRS (France); ASI (Italy); MCINN (Spain); SNSB (Sweden); STFC and UKSA (UK); and NASA (USA). The VISTA magnitude is based on observations collected at the European Organization for Astronomical Research in the Southern hemisphere under ESO programme(s) 179.B-2003.

Facilities: The research is based on the observations with *Herschel* – an ESA space observatory with science instruments provided by European-led Principal Investigator consortia and with important participation from NASA.

REFERENCES

Asplund M., Grevesse N., Sauval A. J., Scott P., 2009, ARA&A, 47, 481
Barlow M. J. et al., 2010, A&A, 518, L138
Bocchio M., Jones A. P., Slavin J. D., 2014, A&A, 570, A32
Bonanos A. Z. et al., 2010, AJ, 140, 416
Bowen G. H., Willson L. A., 1991, ApJ, 375, L53
Boyer M. L. et al., 2010, A&A, 518, L142
Boyer M. L. et al., 2012, ApJ, 748, 40
Choi Y. K. et al., 2008, PASJ, 60, 1007
Cioni M.-R. L. et al., 2011, A&A, 527, A116
Cole A. A., Tolstoy E., Gallagher J. S., III, Smecker-Hane T. A., 2005, AJ, 129, 1465
Davies B. et al., 2013, ApJ, 767, 3
De Beck E., Decin L., de Koter A., Justtanont K., Verhoelst T., Kemper F., Menten K. M., 2010, A&A, 523, A18
Decin L., Hony S., Koter A. D., Justtanont K., Tielens A. G. G. M., Waters L. B. F. M., 2006, A&A, 456, 549
Decin L. et al., 2010, A&A, 521, L4
Dwek E., 1998, AJ, 501, 643
Egan M. P., Van Dyk S., Price S., 2001, AJ, 122, 1844
Elias J. H., Frogel J. A., Schwering P. B. W., 1986, ApJ, 302, 675
France K. et al., 2010, Science, 329, 1624
Gehrz R. D., 1989, in Allamandola L. J., Tielens A. G. G. M., eds, Proc. IAU Symp. 135, Interstellar Dust. Kluwer, Dordrecht, p. 445
Gomez H. L. et al., 2012, ApJ, 760, 96
Gordon K. D. et al., 2014, ApJ, 797, 85
Gotthelf E. V., Koralesky B., Rudnick L., Jones T. W., Hwang U., Petre R., 2001, ApJ, 552, L39
Griffin M. J. et al., 2010, A&A, 518, L3
Groenewegen M. A. T. et al., 2007, MNRAS, 376, 313
Groenewegen M. A. T., Sloan G. C., Soszynski I., Petersen E. A., 2009, A&A, 506, 1277
Höfner S., Dorfi E. A., 1997, A&A, 319, 648
Indebetouw R. et al., 2014, ApJ, 782, L2
Ivezic Z., Elitzur M., 1997, MNRAS, 287, 799
Justtanont K., Tielens A. G. G. M., 1992, ApJ, 389, 400
Karakas A. I., van Raai M. A., Lugaro M., Sterling N. C., Dinerstein H. L., 2009, ApJ, 690, 1130
Kemper F., Stark R., Justtanont K., De Koter A., Tielens A. G. G. M., Waters L. B. F. M., Cami J., Dijkstra C., 2003, A&A, 407, 609
Kemper F. et al., 2010, PASP, 122, 683
Khouri T. et al., 2014a, A&A, 570, A67
Khouri T. et al., 2014b, A&A, 561, A5
Knapp G. R., Morris M., 1985, ApJ, 292, 640
Knapp G. R., Pourbaix D., Platais I., Jorissen A., 2003, A&A, 403, 993
Lagadec E., Zijlstra A. A., Mauron N., Fuller G., Josselin E., Sloan G. C., Riggs A. J. E., 2010, MNRAS, 403, 1331
Lakićević M. et al., 2015, ApJ, 799, 50
Levesque E. M., Massey P., Olsen K. A. G., Plez B., Josselin E., Maeder A., Meynet G., 2005, ApJ, 628, 973
Levesque E. M., Massey P., Plez B., Olsen K. A. G., 2009, AJ, 137, 4744
Loup C., Forveille T., Omont A., Paul J. F., 1993, A&AS, 99, 291
Marshall J. R., van Loon J. T., Matsuura M., Wood P. R., Zijlstra A. A., Whitelock P. A., 2004, MNRAS, 355, 1348
Massey P., Levesque E. M., Plez B., 2006, ApJ, 646, 1203
Mathis J. S., Rumpl W., Nordsieck K. H., 1977, ApJ, 217, 425
Matsuura M. et al., 2009, MNRAS, 396, 918
Matsuura M., Woods P. M., Owen P. J., 2013, MNRAS, 429, 2527
Matsuura M. et al., 2014, MNRAS, 437, 532
Matsuura M. et al., 2015, ApJ, 800, 50
Mauron N., Josselin E., 2011, A&A, 526, A156
McDonald I., Zijlstra A. A., 2014, MNRAS, 446, 2226
Meixner M. et al., 2006, AJ, 132, 2268
Meixner M. et al., 2013, AJ, 146, 62
Meynet G. et al., 2015, A&A, 575, A60
Monnier J. D. et al., 2004, ApJ, 605, 436
Müller H. S. P., Schlöder F., Stutzki J., Winnewisser G., 2005, J. Mol. Struct., 742, 215
Naylor D. A. et al., 2014, in Oschmann J. M., Clampin M., Fazio G. G., MacEwen H. A., eds, Proc. SPIE Conf. Ser. Vol. 9143, In-orbit Performance of the *Herschel*/SPIRE Imaging Fourier Transform Spectrometer: Lessons Learned. SPIE, Bellingham, p. 2
Nozawa T., Kozasa T., Tominaga N., Maeda K., Umeda H., Nomoto K., Krause O., 2010, ApJ, 713, 356
O'Gorman E. et al., 2015, A&A, 573, L1
Ohnaka K., Driebe T., Hofmann K.-H., Weigelt G., Wittkowski M., 2008, A&A, 484, 371
Ossenkopf V., Henning T., 1994, A&A, 291, 943
Ossenkopf V., Henning T., Mathis J. S., 1992, A&A, 261, 567
Ott S., 2010, in Mizumoto Y., Morita K.-I., Ohishi M., eds, ASP Conf. Ser. Vol. 434, Astronomical Data Analysis Software and Systems XIX: The *Herschel* Data Processing System – HIPE and Pipelines – Up and Running Since the Start of the Mission. Astron. Soc. Pac., San Francisco, p. 139

Pietrzynski G. et al., 2013, Nature, 495, 76
Pilbratt G. L. et al., 2010, A&A, 518, L1
Poglitsch A. et al., 2010, A&A, 518, L2
Press W. H., Teukolsky S. A., Vetterling W. T., Flannery B. P., 1992, Numerical Recipes in FORTRAN. The Art of Scientific Computing. Cambridge Univ. Press, Cambridge
Ramstedt S., Schöier F. L., Olofsson H., Lundgren A. A., 2008, A&A, 487, 645
Rawlings J. M. C., Yates J. A., 2001, MNRAS, 326, 1423
Raymond J. C., Ghavamian P., Williams B. J., Blair W. P., Borkowski K. J., Gaetz T. J., Sankrit R., 2013, ApJ, 778, 161
Richards A. M. S., Yates J. A., Cohen R. J., 1998, MNRAS, 299, 319
Riebel D., Srinivasan S., Sargent B. A., Meixner M., 2012, ApJ, 753, 71
Roche P. F., Aitken D. K., Smith C. H., 1993, MNRAS, 262, 301
Royer P. et al., 2010, A&A, 518, L145
Rubele S. et al., 2015, MNRAS, 449, 639
Rybicki G. B., Hummer D. G., 1991, A&A, 245, 171
Sargent B. A. et al., 2010, ApJ, 716, 878
Scharmer G. B., Carlsson M., 1985, J. Comput. Phys., 59, 56
Silvia D. W., Smith B. D., Shull J. M., 2010, ApJ, 715, 1575
Skrutskie M. F. et al., 2006, AJ, 131, 1163
Sloan G. C., Kraemer K. E., Wood P. R., Zijlstra A. A., Bernard-Salas J., Devost D., Houck J. R., 2008, ApJ, 686, 1056
Smartt S. J., 2009, ARA&A, 47, 63
Smith N., Humphreys R. M., Davidson K., Gehrz R. D., Schuster M. T., Krautter J., 2001, AJ, 121, 1111
Srinivasan S. et al., 2009, AJ, 137, 4810
Swinyard B. M. et al., 2010, A&A, 518, L4
Swinyard B. M. et al., 2014, MNRAS, 440, 3658
Temim T., Dwek E., Tchernyshyov K., Boyer M. L., Meixner M., Gall C., Roman-Duval J., 2015, ApJ, 799, 158
Tielens A. G. G. M., 2010, The Physics and Chemistry of the Interstellar Medium. Cambridge Univ. Press, Cambridge
Ueta T., Meixner M., 2003, ApJ, 586, 1338
van den Bergh S., 2000, The Galaxies of the Local Group. Cambridge Univ. Press, Cambridge
van Loon J. T., Groenewegen M. A. T., De Koter A., Trams N. R., Waters L. B. F. M., Zijlstra A. A., Whitelock P. A., Loup C., 1999, A&A, 351, 559
van Loon J. T., Zijlstra A. A., Bujarrabal V., Nyman L., 2001, A&A, 368, 950
van Loon J. T., Cioni M.-R. L., Zijlstra A. A., Loup C., 2005a, A&A, 438, 273
van Loon J. T., Marshall J. R., Zijlstra A. A., 2005b, A&A, 442, 597
Vassiliadis E., Wood P. R., 1993, ApJ, 413, 641
Wachter A., Winters J. M., Schröder K.-P., Sedlmayr E., 2008, A&A, 486, 497
Weaver T. A., Woosley S. E., 1980, Ann. New York Acad. Sci., 336, 335
Willacy K., Millar T. J., 1997, A&A, 324, 237
Wood P. R., Bessell M. S., Whiteoak J. B., 1986, ApJ, 306, L81
Wood P. R., Whiteoak J. B., Hughes S. M. G., Bessell M. S., Gardner F. F., Hyland A. R., 1992, ApJ, 397, 552
Yang B., Stancil P. C., Balakrishnan N., Forrey R. C., 2010, ApJ, 718, 1062

This paper has been typeset from a TEX/LATEX file prepared by the author.